ELSEVIER

Journal of Marine Systems 8 (1996) 237–254

JOURNAL OF MARINE SYSTEMS

# Advection schemes for shelf sea models

I.D. James

*Proudman Oceanographic Laboratory, Bidston Observatory, Birkenhead, L43 7RA, UK*

Received 8 October 1994; accepted 5 August 1995

**Abstract**

Numerical models of shelf seas must handle sharp gradients in thermoclines and fronts, and at the edges of patches of passive tracer, often in the presence of strong tidal currents, without introducing excessive numerical diffusion or spurious oscillations. In a sigma coordinate model there is an additional problem, since then purely horizontal motion over a sloping sea bed may introduce strong numerical diffusion in the vertical, which can artificially erode thermoclines.

In this paper, two advection schemes applicable to shelf sea models are examined. They are based on TVD (Total Variation Diminishing) and PPM (Piecewise Parabolic Method) techniques. They are demonstrated to give satisfactory performance for tracer advection in one, two and three dimensions. They are both monotonic, and the PPM scheme has particularly low numerical diffusion. In two and three dimensions directional splitting is used, which is handled by following advection with each horizontal velocity component by adjustment of the sigma levels in each water column using the same advection scheme. The artificial vertical diffusion is then small, particularly with PPM.

The two schemes are also compared in a three-dimensional model of a cylindrical eddy of relatively fresh water, released from rest in an open sea region. Here, both salinity and momentum are advected. Laboratory experiments show that after an initial period of adjustment the eddy should become unstable, with a growth of cyclonic–anticyclonic eddy pairs. This is reproduced in the model, with the PPM scheme again producing sharper results than the TVD scheme.

Integrated second moment calculations are used to compare the schemes. These demonstrate the lower numerical diffusion of the PPM scheme. This advantage is achieved at the cost of greater computing time.

## 1. Introduction

In the simplest one-dimensional case, the equation for the advection of a variable $a(x,t)$ by a constant velocity $u$ is

$$\partial a/\partial t = -u\partial a/\partial x \tag{1}$$

or, in flux form,

$$\partial a/\partial t = -\partial(ua)/\partial x \tag{2}$$

It is well known (see, for example, Press et al., 1992) that the forward time step, centred space step (FTCS) finite difference method for the solution of this equation, namely

$$a_i^{n+1} = a_i^n - u\Delta t(a_{i+1}^n - a_{i-1}^n)/2\Delta x \tag{3}$$

is unconditionally unstable, but that if the flux $F_{i+\frac{1}{2}} = u(a_i^n + a_{i+1}^n)/2$ used in the FTCS method is replaced by

$$u(a_i^n + a_{i+1}^n)/2 + u^2\Delta t(a_i^n - a_{i+1}^n)/2\Delta x \tag{4}$$

giving the Lax-Wendroff method, there is stability if


*PII* S0924-7963(96)00008-5

$|u|\Delta t \leq \Delta x$ (the Courant-Friedrichs-Lewy, or CFL, condition). Also, if this flux is replaced by

$$u(a_i^n + a_{i+1}^n)/2 + |u|(a_i^n - a_{i+1}^n)/2 \qquad (5)$$

we have upwind differencing, which is also stable if the CFL condition is satisfied.

One reason there is an extensive and growing literature on the numerical solution of the advection equation is that neither of these methods is satisfactory when sharp gradients, and that means a spatial scale of less than several grid intervals, have to be modelled. This is a requirement for many geophysical flows, which include density currents, fronts and thermoclines and for the advection of any constituent with sharp concentration gradients, for example sediment or a pollutant. The correct representation of fronts and thermoclines is important also for biological models. The particular application of interest in this paper is the advection of fronts and thermoclines in shelf seas.

The drawback to the Lax-Wendroff method (4) is that it lacks positivity, and produces spurious ripples in the solution near a sharp front. First-order upwind differencing (5), on the other hand, though positive, is highly diffusive, with a diffusion coefficient (Smolarkiewicz 1983) equal to $(u\Delta x - \Delta t u^2)/2$. Advection by strong tidal currents would destroy a sharp front after a few tidal cycles in a model using this scheme.

Several solutions to the problem have been proposed. Notable among these have been flux-corrected transport (FCT, Boris and Book, 1976), the self-adjusting hybrid scheme (SAHS, Harten, 1978), the antidiffusive velocity method (Smolarkiewicz, 1983), total variation diminishing (TVD) schemes (Harten, 1983, Sweby, 1984), the monotonic upwind schemes of van Leer, for example MUSCL (Van Leer, 1979), and the piecewise parabolic method (PPM, Colella and Woodward, 1984).

We may follow Yang and Przekwas (1992) in dividing most of these into algebraic schemes and geometric schemes. The algebraic schemes are basically hybrid schemes, in which the total flux is taken to be a sum of contributions from a low-order diffusive scheme, for example first-order upwind, and from a higher order dispersive scheme, for example Lax-Wendroff. The methods differ in the way they calculate the proportion of the contribution from each scheme. The SAHS method, which has been used in the context of shelf sea fronts and eddies (James, 1986), applies more of the diffusive scheme when the edge of fronts is detected, but includes adjustable parameters. The FCT method uses a predictor–corrector technique to ensure that no new extrema are produced in the solution, so that there is no spurious rippling near fronts. It is possible to prove sufficient conditions on the proportionality coefficients to ensure TVD, or ripple-free, behaviour (Sweby, 1984). Some of the resulting limiter functions satisfying the TVD conditions give sharper results than others (Yang and Przekwas, 1992). The geometric schemes essentially construct a variation of the advected variable within each grid cell, which may be kept monotonic so that no spurious extrema are produced. The interface flux may be calculated by an upstream method. The lowest order version of this method would have no variation within each cell, and the first-order upwind scheme would be recovered. Linear variation within each cell may be used (Van Leer, 1979), and PPM has parabolic variation. There remains a discontinuity in the variable at the boundary of each grid cell as the function is only piecewise parabolic. For a compressible flow, these can be taken as actual discontinuities, and the resulting interface flux can be found by solving a Riemann problem (Colella and Woodward, 1984). The PPM scheme for compressible flow has been applied to meteorological problems (Carpenter et al., 1990), although the compressibility, which allows shocks and sound waves, severely limits the time step. In this paper, applications are restricted to incompressible flow. Results will be shown for two methods, one algebraic and one geometric, which have been shown in several examples (Roe, 1986; Carpenter et al., 1990; Yang and Przekwas, 1992) to perform well, namely, a TVD scheme and PPM.

In this paper we consider a sigma coordinate system in the vertical, in which the cartesian vertical coordinate $z$, which has the value $\zeta(x,y,t)$ of the elevation at the sea surface and the value $-h(x,y)$ at the sea bed, is transformed by

$$\sigma = (z - \zeta)/(h + \zeta) \qquad (6)$$

so that $\sigma$ is always zero at the surface and $-1$ at the

bed. Therefore the sigma coordinates follow the surface and bed and it is possible to include the effects of frictional boundary layers there much more easily than with $z$ coordinates. A disadvantage of sigma coordinates is that they are inclined to the horizontal, especially over steep bathymetry, so that horizontal advection which would be entirely in the $x$ direction in $(x,z)$ coordinates becomes inclined to the grid in $(x,\sigma)$ coordinates. It is easy to see, then, that an excessively diffusive advection scheme applied to advection which is predominantly horizontal can introduce spurious vertical diffusion. In extreme cases, such as the continental slope, more than one layer each transformed into sigma coordinates may be adopted (Beckers, 1991), but only one on the shelf will be considered here. Three-dimensional advection may be handled by means of directional splitting, so that each direction in turn is covered by a one-dimensional routine. In practice, the requirements to take care of volume conservation and sigma coordinates mean that in a three-dimensional code advection in the $x$ direction followed by vertical adjustment is followed by advection in the $y$ direction followed by a second vertical adjustment.

## 2. A TVD scheme

The TVD scheme used here, due to Roe (1986) and Sweby (1984), is based on a combination of the first-order upwind and Lax-Wendroff schemes so that

$$\text{total flux } F_{i+\frac{1}{2}} = F^{\mathrm{UP}}_{i+\frac{1}{2}} + \phi(r)\left(F^{\mathrm{LW}}_{i+\frac{1}{2}} - F^{\mathrm{UP}}_{i+\frac{1}{2}}\right) \tag{7}$$

where $F^{\mathrm{UP}}$ and $F^{\mathrm{LW}}$ are the fluxes given by the upwind and Lax-Wendroff schemes. The function $\phi(r)$ is a limiter function depending on the behaviour of $a$: we take, equivalent to equation (2.15) of Yang and Przekwas (1992),

$$r = F^{\mathrm{LMU}}_{i+\frac{1}{2}-s} \Big/ F^{\mathrm{LMU}}_{i+\frac{1}{2}} \tag{8}$$

where

$$F^{\mathrm{LMU}}_{i+\frac{1}{2}} = F^{\mathrm{LW}}_{i+\frac{1}{2}} - F^{\mathrm{UP}}_{i+\frac{1}{2}} \tag{9}$$

$$= \left(\left|u_{i+\frac{1}{2}}\right| - \Delta t u^2_{i+\frac{1}{2}} \Big/ \Delta x\right)(a_{i+1} - a_i)/2 \tag{10}$$

and

$$s = \operatorname{sign}\left(u_{i+\frac{1}{2}}\right) \tag{11}$$

If $F^{\mathrm{LMU}}_{i+\frac{1}{2}} = 0$, we take $r = 0$, but then Eq. (7) gives, for any finite $\phi(r)$, $F_{i+\frac{1}{2}} = F^{\mathrm{UP}}_{i+\frac{1}{2}} = F^{\mathrm{LW}}_{i+\frac{1}{2}}$.

Several limiter functions have the TVD property (Sweby, 1984, Roe, 1986, Yang and Przekwas, 1992). These include:

$$\text{Minimod: } \phi(r) = \max(0, \min(1, r)) \tag{12}$$

$$\text{Monotonic: } \phi(r) = (r + |r|)/(1 + r) \tag{13}$$

$$\text{MUSCL: } \phi(r) = \max(0, \min(2, 2r, (1 + r)/2)) \tag{14}$$

$$\text{Superbee: } \phi(r) = \max(0, \min(2r, 1), \min(r, 2)) \tag{15}$$

These differ in the sharpness of the results. Examples are given here using the superbee limiter, which is reported (Sweby, 1984; Roe, 1986; Yang and Przekwas, 1992) to be one of the least diffusive, although it can sometimes produce artificial steepening.

## 3. The piecewise parabolic method

As described in the introduction, PPM, taking the values of a variable at the beginning of a time step to be the mean values of that variable within a grid box, constructs a parabolic variation of the variable within the grid box. This parabola may be determined by three parameters, the mean value $\bar{a}$ (which remains equal to $a_i^n$) and its values $a_{\mathrm{L}}$ and $a_{\mathrm{R}}$ at the left and

right edges of the grid interval. If the variable $\xi = \left(x - x_{i-\frac{1}{2}}\right)/\Delta x$, which runs from 0 to 1 within the interval, the parabola is

$$a(\xi) = a_L + \xi(a_R - a_L + a_6(1 - \xi)) \quad (16)$$

where

$$a_6 = 6\bar{a} - 3(a_L + a_R) \quad (17)$$

It remains to find the values $a_L$ and $a_R$ at the zone edges. The details are given by Colella and Woodward (1984) and will not be repeated here. The first guess, from a polynomial fit, assumes a common edge value

$$a_{i+\frac{1}{2}} = a_{R,i} = a_{L,i+1} \quad (18)$$

The optional process of steepening may then be applied. This helps retain the steepness of discontinuities in the solution. A discontinuity is deemed to occur if the third derivative is large, if the second derivative changes sign and the first and third derivatives have opposite signs. Steepening involves adjustable parameters: the same values as used by Colella and Woodward (1984) are used here. Use of the steepener is appropriate when discontinuous fronts and shocks are considered, but should be used with caution as artificial steepening can sometimes occur (Carpenter et al., 1990).

Near boundaries, there are not enough neighbouring points to determine parabolas. They reduce to constant values, equal to the zone average $a_i$, at or next to the boundary, and linear slopes at the next point away from the boundary.

The final stage in determining the parabolas is monotonisation, forcing the parabola to take values lying between $a_L$ and $a_R$. Then the advective fluxes out of each zone cannot produce new extrema.

## 4. Directional splitting and sigma coordinates

Once the parabolas for the PPM scheme have been determined, values of the advective fluxes can be calculated. These take the form of definite integrals of the parabolas from the appropriate grid box edge to some point within the grid box. For the case of one dimension and constant velocity $u > 0$, the range of integration in $x$ for flux $F_{i+\frac{1}{2}}$ is clearly from $x_{i+\frac{1}{2}} - u\Delta t$ to $x_{i+\frac{1}{2}}$. The CFL condition ensures that $u\Delta t < \Delta x$. Fig. 1 shows the more general case of advection across a vertical face into a water column in sigma coordinates. Here, the volume flow, per unit length in the $y$ direction, out of a grid box face in time $\Delta t$ must first be calculated by any appropriate method, and then the range of integration of the parabola is given by that volume divided by the height of the grid box.

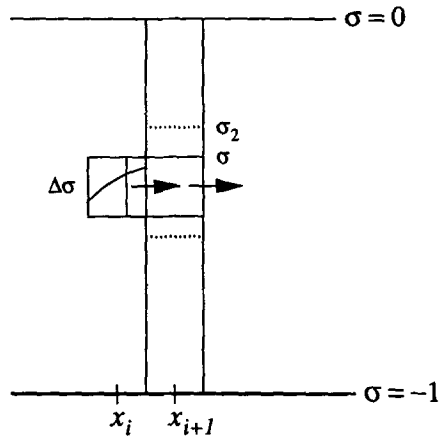


Fig. 1. Fluxes into a vertical column in sigma coordinates.

For example, if $H_{i+\frac{1}{2}}$ is the total depth at $x_{i+\frac{1}{2}}$, where velocity $u_{i+\frac{1}{2}}$ is defined, and $H_i$ is the depth at $x_i$, where the variable $a_i$ is defined, the volume flux per unit length in time $\Delta t$ across a vertical grid box face at $x_{i+\frac{1}{2}}$ is

$$H_{i+\frac{1}{2}}\, u_{i+\frac{1}{2}}\, \Delta\sigma\Delta t \quad (19)$$

If $u_{i+\frac{1}{2}} > 0$, the height, defined as volume per unit length divided by $\Delta x$, of the grid box from which this volume is taken is $H_i\Delta\sigma$. Therefore the appro-

priate range of integration of the parabola within this box, giving the flux of the variable $a$, is from $x_{i+\frac{1}{2}} - \left(H_{i+\frac{1}{2}} u_{i+\frac{1}{2}} \Delta t\right)/H_i$ to $x_{i+\frac{1}{2}}$.

Hence, the PPM scheme can be used to give fluxes of the variable $a$ across vertical faces. We have already seen how the TVD scheme can also be used to give these fluxes. In a two or three-dimensional problem we need to follow this by advection in the vertical. In sigma coordinates, the transformed vertical velocity becomes, for two dimensions,

$$\Omega = -(\sigma/H)\partial\zeta/\partial t - (1/H)\partial\left(H\int_0^\sigma u\,\mathrm{d}\sigma\right)\Big/\partial x \tag{20}$$

This is always zero at the surface and sea bed. Although it would be possible to perform advection in the vertical directly using values of $\Omega$ calculated

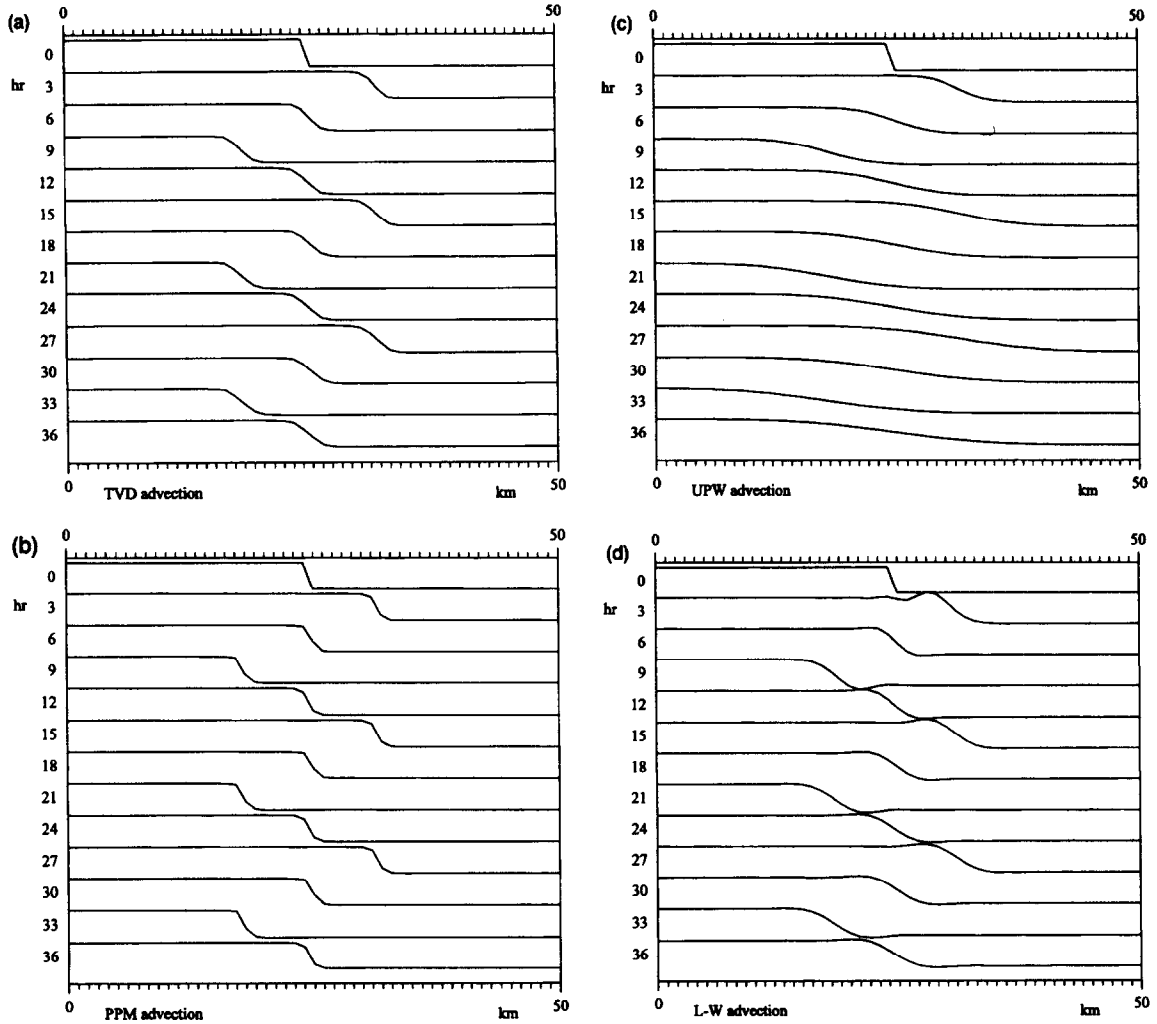


Fig. 2. One-dimensional advection of a discontinuity by an oscillatory current with period 12 hours: (a) TVD scheme with superbee limiter, (b) PPM scheme with steepening, (c) upwind scheme, (d) Lax-Wendroff scheme.

from (20), here we do an equivalent calculation using the volume fluxes across vertical faces, which have already been needed to find the range of integration for the parabolas in the PPM scheme.

Consider the horizontal volume fluxes into a single vertical column (Fig. 1). The total flux integrated over the depth determines the change in elevation $\zeta$, while the variation of fluxes with depth determines a change in sigma level of the upper and lower faces of each grid box in the column if volumes are to be conserved. Therefore once the flux of the variable $a$ across the vertical faces has been determined by either method we have values of the advected variable in each grid box in the vertical column, but with a new intermediate distribution of the sigma levels of the upper and lower grid box faces shown in Fig. 1 by the dotted lines and labelled $\sigma_2$. Then the problem of vertical advection reduces to a readjustment of these intermediate sigma levels back to the original distribution. For the PPM scheme, new parabolas representing the vertical variation in each column must be determined for the intermediate intervals in sigma. The range of integration of the parabolas determining the fluxes which correspond to a readjustment to the original sigma levels is now simply the difference between the intermediate and original sigma level of each face. For the TVD method the readjustment of the sigma levels involves a Lax-Wendroff scheme generalised for unequal intervals.

When the advection routine is used as part of a two or three-dimensional model, elevation $\zeta$ may be calculated in another part of the model, typically in a subroutine concerning barotropic depth-integrated flow, probably on a different time step, possibly by a different method. Then the calculation of $\zeta$ in the advection step may be considered as giving a separate, temporary value having the important function of ensuring conservation within the advection routine.

Because of the inclination of sigma coordinate surfaces to the horizontal, advection by a horizontal velocity causes transfer from one sigma grid box to another in a vertical column, and this is handled by the vertical readjustment process as described above. If the scheme is not sharp enough, unwanted diffusion of a thermocline can occur. In three dimensions, with directional splitting, vertical adjustment must follow each of the two horizontal advection steps, so that all columns have the same distribution of sigma levels at the beginning of each horizontal step. The sigma grid intervals in this distribution need not be equal, so there could be a concentration at regions of interest, such as the surface, sea bed, or thermocline depth. The order of the horizontal steps is reversed on alternate time steps to avoid asymmetry.

## 5. Advection in one and two dimensions

### 5.1. One-dimensional performance

The one-dimensional performance of the schemes discussed here is demonstrated in Fig. 2. These all show the advection of an initial sharp discontinuity of width one grid interval by an oscillatory tidal current. The grid interval $\Delta x$ is 1 km and the current has a period of 12 hr and an amplitude of 1 m $s^{-1}$. Both the TVD scheme (Fig. 2a), with superbee limiter, and the PPM scheme (Fig. 2b), with steepening, retain a sharp front with monotonic behaviour. The PPM scheme is sharper, with 69% of the jump still within one grid interval and 98% within 3 intervals after three tidal cycles. For the TVD scheme, 82% of the jump is within 3 intervals and 97% within 5 intervals after three tidal cycles and there is only very slight diffusion between the second and third cycle. The results at the end of the third tidal cycle for the PPM scheme are identical to those at the end of the second cycle to 4 significant figures: negligible diffusion is occurring for PPM. For comparison the upwind scheme (Fig. 2c) and the Lax-Wendroff scheme (Fig. 2d) are also shown. These are clearly unsatisfactory for the reasons anticipated in the introduction: the upwind scheme is excessively diffusive, and the Lax-Wendroff scheme produces spurious oscillations giving values greater than the original maximum and less than the original minimum in the front. These oscillations are worse near the beginning, being still obvious in the 3 hr result, but the inherent diffusive behaviour of the Lax-Wendroff scheme, particularly for the shorter wavelengths, damps them out as the tidal oscillations continue. At 36 hours, spurious values with amplitude 5% of the original jump remain, while 94% of the jump has been spread over 5 grid intervals.

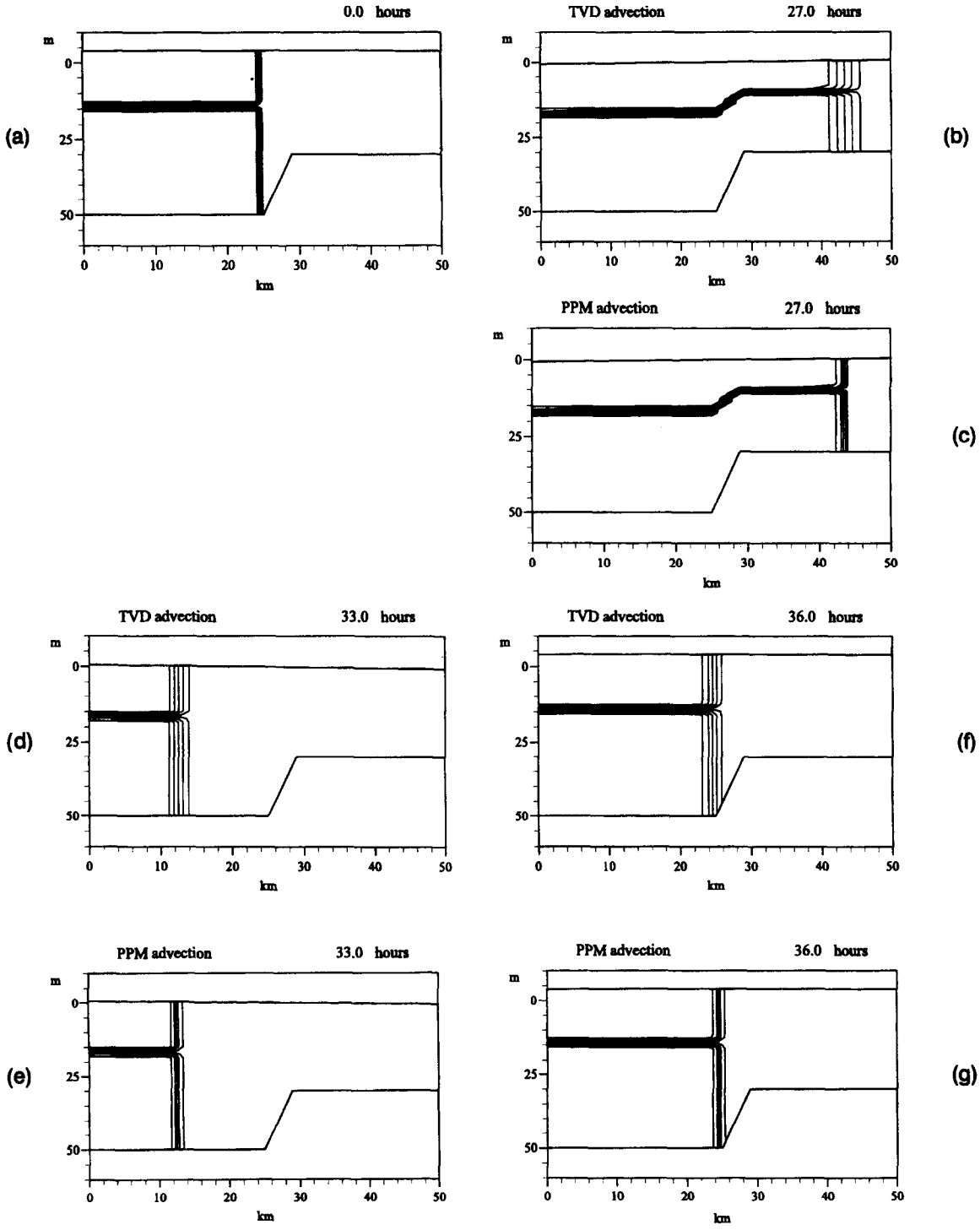


Fig. 3. Advection of a front between stratified and homogeneous fluid by a 12 hour progressive wave over a slope: (a) initial condition: contours are from −0.9 to 0.9 with an interval of 0.2, (b) the TVD scheme at 27 hours, (c) the PPM scheme at 27 hours, (d) the TVD scheme at 33 hours, (e) the PPM scheme at 33 hours, (f) the TVD scheme at 36 hours, (g) the PPM scheme at 36 hours.

Table 1
Values of integrated second moment $I$

| *One-dimensional (section 5.1)* | | | | | | |
|---|---|---|---|---|---|---|
| Hours | 12 | 24 | 36 | | | |
| upwind | 0.8999 | 0.8572 | 0.8207 | | | |
| Lax-Wendroff | 0.9833 | 0.9797 | 0.9773 | | | |
| TVD | 0.9763 | 0.9748 | 0.9742 | | | |
| PPM | 0.9886 | 0.9886 | 0.9886 | | | |
| *Two-dimensional over slope (section 5.3)* | | | | | | |
| Hours | 12 | 24 | 36 | | | |
| TVD | 0.9548 | 0.9499 | 0.9475 | | | |
| PPM | 0.9758 | 0.9754 | 0.9754 | | | |
| *Three-dimensional tracer (section 6.2)* | | | | | | |
| Hours | 6 | 12 | 18 | 24 | | |
| TVD | 0.6682 | 0.6004 | 0.5489 | 0.5137 | | |
| PPM | 0.8622 | 0.8427 | 0.8212 | 0.8183 | | |
| *Three-dimensional eddy (section 6.3)* | | | | | | |
| Days | 1 | 2 | 3 | 4 | 5 | 6 |
| upwind | 0.3454 | 0.2720 | 0.2334 | 0.2078 | 0.1870 | 0.1688 |
| Lax-Wendroff | 0.9326 | 0.9090 | 0.8922 | 0.8723 | 0.8471 | 0.8291 |
| TVD | 0.5976 | 0.5840 | 0.5732 | 0.5506 | 0.4946 | 0.4213 |
| PPM | 0.6849 | 0.6774 | 0.6735 | 0.6493 | 0.5807 | 0.4970 |

Another measure of numerical diffusion is the integrated second moment

$$I = \int a(t)^2 \, dV / \int a(0)^2 \, dV \qquad (21)$$

where the integrals are taken over the whole domain, and $a(t)$ represents the variable concerned at time $t$. For pure advection with no sources or sinks, $I$ would remain equal to 1 for all $t > 0$. The rate of decrease of $I$ provides a measure for the amount of numerical diffusion. Table 1 gives the results of second moment calculations for the examples given here. For the one-dimensional cases just described there are sources and sinks at the open boundaries, so a comparison can be given only after each complete tidal cycle, and the actual values depend on the length of the domain. The results show the relatively high diffusion of upwind compared with the other schemes and the lack of diffusion in PPM after the first tidal cycle. PPM is less diffusive than TVD. The Lax-Wendroff scheme gives higher values than TVD, but the value of $I$ is increased by the dispersive ripples.

In all these runs, a forward time step of 360s was used, giving a maximum Courant number $|u|\Delta t/\Delta x = 0.36$. These schemes are limited by the CFL condition, Courant number $\leq 1$, unlike for example the SHARP scheme (Leonard, 1988), which has a more stringent condition on Courant number.

### 5.2. Advection in two dimensions by a progressive oscillatory wave

The one-dimensional results show that the PPM and TVD schemes have the behaviour necessary for models which include sharp fronts and thermoclines and strong advective currents. As discussed in a previous section, the adaptation of the one-dimensional schemes to a two-dimensional (one horizontal, one vertical) sigma-coordinate model is not trivial. However, a return to $z$ coordinates is not a complete answer to excess vertical diffusion of thermoclines: there are many likely flows in which the natural flow direction is not horizontal. The flow is more nearly along the sigma coordinate direction near a sloping sea bed. It is easy to devise a flow field which is along sigma coordinates everywhere, based on advection by a progressive oscillatory wave over a slope. With the assumption of a velocity uniform with depth and a given sinusoidal elevation, continuity implies vertical velocities. These vertical velocities of course cross the horizontal $z$-levels but not, in this case, the sigma levels. For the flow over the slope, currents in the shallower water are greater than currents on the deep side and water is drawn up the slope. This upslope flow would pose more problems for $z$ coordinates than for sigma coordinates: the simple case for $z$ coordinates, a purely horizontal flow which crosses the sigma coordinate levels, is considered in the next sub-section.

The initial condition for these runs is a front between stratified and vertically homogeneous tracer,

Fig. 4. Advection of a surface front over a slope, across sigma surfaces, by a uniform 12 hour oscillatory horizontal velocity in the top 30 m: (a) initial condition: contours are from 0.1 to 0.9 with an interval of 0.2, (b) the TVD scheme at 27 hours, (c) the PPM scheme at 27 hours, (d) the TVD scheme at 33 hours, (e) the PPM scheme at 33 hours, (f) the TVD scheme at 36 hours, (g) the PPM scheme at 36 hours.

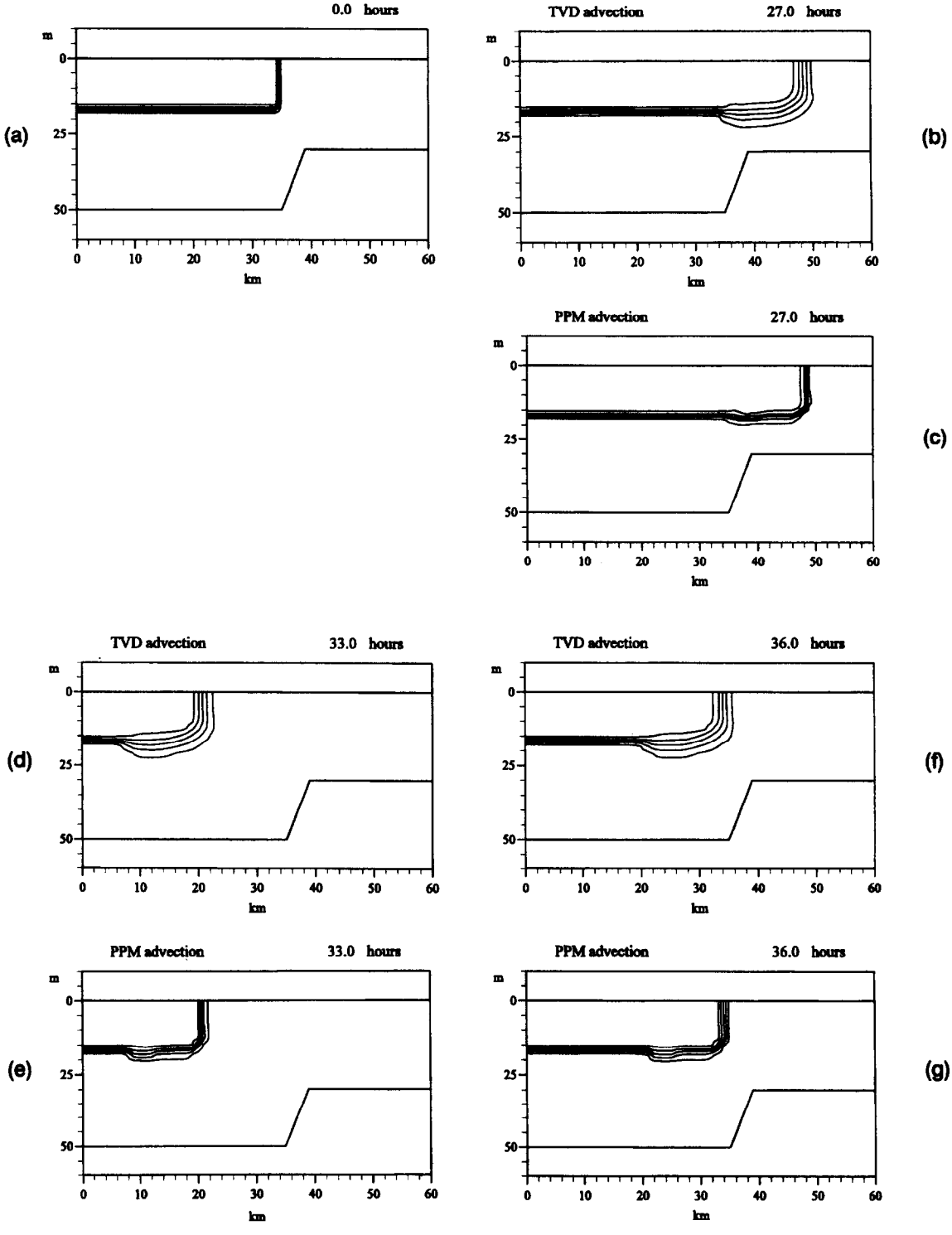
(a)
0.0 hours
m
0
25
50
0 10 20 30 40 50 60
km
(b)
TVD advection
27.0 hours
m
0
25
50
0 10 20 30 40 50 60
km
(c)
PPM advection
27.0 hours
m
0
25
50
0 10 20 30 40 50 60
km
(d)
TVD advection
33.0 hours
m
0
25
50
0 10 20 30 40 50 60
km
(f)
TVD advection
36.0 hours
m
0
25
50
0 10 20 30 40 50 60
km
(e)
PPM advection
33.0 hours
m
0
25
50
0 10 20 30 40 50 60
km
(g)
PPM advection
36.0 hours
m
0
25
50
0 10 20 30 40 50 60
km

here given the values 1, 0 and −1, and with discontinuous jumps over one grid box in both horizontal and vertical directions. The figures show, for both TVD (superbee) and PPM (with steepener) schemes, the state after three 12 hour tidal cycles at 36 hours, together with the state at the two previous extreme tidal excursions at 27 and 33 hours. The horizontal grid interval $\Delta x$ is 1 km, while there are 20 sigma levels in the vertical, hence 18 grid intervals between surface and sea bed.

Fig. 3 shows the results for a bottom with a steep slope, 4 grid intervals long, from 50 to 30 m, and an imposed wave elevation amplitude of 4 m and phase velocity 22 m $s^{-1}$. These results follow the behaviour to be expected after seeing the one-dimensional runs: the front is maintained in both schemes despite repeated advection over many grid intervals, with PPM giving somewhat sharper results than TVD. The thermocline is not diffused at all since with this flow field it follows sigma levels: there is an upslope flow along sigma contours on and off the shallow area with each tide.

### 5.3. Advection by a horizontal velocity across sigma levels

In this case we consider a surface front only, between tracer values 1 and 0, advected with a given oscillatory horizontal velocity. The same slope as in Fig. 3 is considered, but the velocity is confined to the upper 30 m, so that for a velocity uniform with horizontal position there is no effect on the surface elevation. In the case shown here, a 12 hour oscillation with amplitude 2 m $s^{-1}$ is imposed. Fig. 4 shows that the thermocline is maintained although the front has crossed several inclined sigma levels. Vertical diffusion is small in both PPM and TVD schemes but less for PPM. Note that the domain has been extended so that the thermocline at the extreme left never reaches the sloping region during the tidal cycles so is not vertically diffused at all. The second moment calculations (Table 1) show that TVD is more diffusive than PPM, and also that the value of $I$ for PPM is the same after the third cycle as it is after the second. In fact the PPM result overall shows very little change between the second and third cycles.

This scheme also gives satisfactory results when the depth change occurs in as little as two grid intervals, but not for one grid interval, which gives instability, when the time step is 180 s. To see why this may be so, we can postulate a variant of the CFL condition based on the fact that the horizontal flux into a grid box cannot influence more than neighbouring sigma grid boxes above and below within one time step. If the sigma coordinates are too steep, a strong enough horizontal flow could reach more sigma levels than this in one time step. So, if the sigma coordinate slope is $s$, we need

$$|\Delta z/s| > |u\Delta t| \tag{22}$$

where $\Delta z$ is the vertical grid interval. If $s = \Delta h/\Delta x$, the Courant number

$$|u\Delta t/\Delta x| < |\Delta z/\Delta h| \tag{23}$$

an additional condition if $|\Delta z/\Delta h| < 1$, that is, if the change in height of the sigma surface in one horizontal grid interval is greater than the vertical distance between sigma levels.

## 6. Application to a three-dimensional hydrodynamic model

### 6.1. Outline of the model

The model used here is based on that of James (1986), but with several changes. The time stepping is now forward rather than leapfrog and the separation into barotropic and baroclinic parts is different: here it is the depth-mean velocities which are calculated with the shorter barotropic time step. A two-dimensional ($x - \sigma$) version of the present model with TVD advection has been used by Souza and James (1996).

The Arakawa B grid is retained as in James

Fig. 5. Advection of a cylinder of tracer in three dimensions by a 12 hour Sverdrup wave, using TVD advection: (a) initial tracer value, (b) surface value at 3 hours, (c) surface value at 6 hours, (d) surface value at 9 hours, (e) surface value at 12 hours, (f) surface value at 24 hours, (g) section through the centre of the tracer ($x = 14$ km) at the initial time, (h) section at $x = 14$ km at 24 hours.

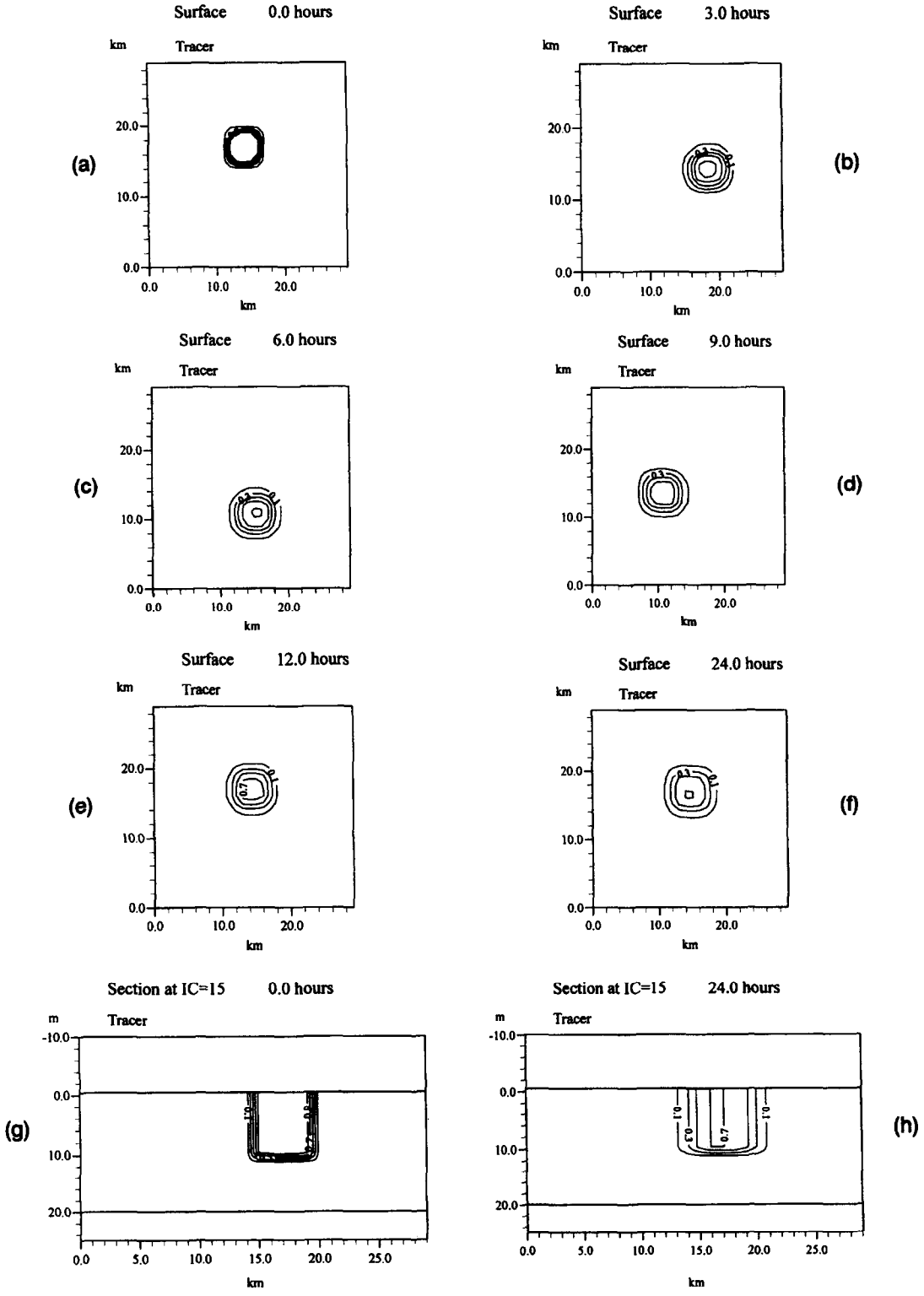
Surface 0.0 hours
Surface 3.0 hours
Surface 6.0 hours
Surface 9.0 hours
Surface 12.0 hours
Surface 24.0 hours
Section at IC=15 0.0 hours
Section at IC=15 24.0 hours
Tracer
km
m
(a)
(b)
(c)
(d)
(e)
(f)
(g)
(h)

(1986). Here, the grid-splitting suppressor of Killworth et al. (1991) has been used to damp out any "checkerboard" behaviour, sometimes found with the B grid, but this was not a problem in the applications shown in this paper.

The incompressible, Boussinesq, hydrostatic equations to be solved on this grid in sigma coordinates ($\alpha = x$, $\beta = y$, $\tau = t$, $\sigma$ defined as in Eq. (6)) are as follows, firstly for the depth mean velocity $(\bar{u}, \bar{v})$:

$$\partial\bar{u}/\partial\tau = f\bar{v} - g\partial\zeta/\partial\alpha + (F_S - F_B)/H + NLB_\alpha \quad (24)$$

$$\partial\bar{v}/\partial\tau = -f\bar{u} - g\partial\zeta/\partial\beta + (G_S - G_B)/H + NLB_\beta \quad (25)$$

$$\partial\zeta/\partial\tau = -\partial(H\bar{u})/\partial\alpha - \partial(H\bar{v})/\partial\beta \quad (26)$$

where $F_S$, $F_B$, $G_S$, $G_B$ are components of surface and bottom stress, $H = h + \zeta$ and $NLB_\alpha$, $NLB_\beta$ are depth means of the non-linear and buoyancy terms in the following equations for velocity deviations $u_r = u - \bar{u}$, $v_r = v - \bar{v}$:

$$\begin{aligned}\partial u_r/\partial\tau = {} & -L(u) + fv_r - \partial\left(H\int_0^\sigma b\,\mathrm{d}\sigma\right)/\partial\alpha \\ & + (\partial\zeta/\partial\alpha + \sigma\partial H/\partial\alpha)\,b \\ & + (1/H^2)\partial(A\partial u/\partial\sigma)/\partial\sigma \\ & - (F_S - F_B)/H - NLB_\alpha \end{aligned} \quad (27)$$

$$\begin{aligned}\partial v_r/\partial\tau = {} & -L(v) - fu_r - \partial\left(H\int_0^\sigma b\,\mathrm{d}\sigma\right)/\partial\beta \\ & + (\partial\zeta/\partial\beta + \sigma\partial H/\partial\beta)\,b \\ & + (1/H^2)\partial(A\partial v/\partial\sigma)/\partial\sigma \\ & - (G_S - G_B)/H - NLB_\beta \end{aligned} \quad (28)$$

Also the salinity $S$ is given by

$$\partial S/\partial\tau = -L(S) + (1/H^2)\partial(K\partial S/\partial\sigma)/\partial\sigma \quad (29)$$

with a similar equation for temperature, where $L$ represents the advective terms. $A$ is the vertical eddy viscosity and $K$ the vertical eddy diffusivity. The buoyancy $b = g(\rho_0 - \rho)/\rho_0$, with $\rho_0$ a reference density.

For the applications shown in this paper, the model is run in frictionless mode, so $F_S$, $F_B$, $G_S$, $G_B$, $A$ and $K$ are all zero. This is possible because the advection schemes retain enough numerical diffusion to prevent a build-up of energy at the grid scale caused by nonlinearity, without producing excessive diffusion of gradients. A frictionless run is a good test of this non-oscillatory behaviour, which does not rely on artificial mixing coefficients.

The barotropic Eq. (24)–(26) are solved by the forward-backward time, centred space scheme, using updated velocities at each stage. Time splitting (Press et al., 1992) is adopted for the baroclinic Eq. (27)–(29), so the terms in the equations are done sequentially. Open boundary conditions are applied to surface elevation and scalars (salinity, temperature and tracer) in a four-point-wide relaxation zone (James, 1990), where values of elevation are made to tend towards the imposed tidal elevation and scalars are made to tend to given boundary values. The velocity is linearised in the column next to the open boundary, so advection of velocity is not applied there.

### 6.2. Advection of a tracer by a tidal current in three dimensions

In this section, the three-dimensional model is applied to a flat-bottomed open sea area with initial and open boundary conditions given by a Sverdrup wave, for which

$$\zeta = Z\cos(kx - \omega t) \quad (30)$$

$$u = g\omega Zk\cos(kx - \omega t)/(\omega^2 - f^2) \quad (31)$$

and

$$v = gfZk\sin(kx - \omega t)/(\omega^2 - f^2) \quad (32)$$

where $\omega$ is the frequency and

$$k^2 = (\omega^2 - f^2)/gh \quad (33)$$

This gives a tidal ellipse with major and minor axes

Fig. 6. Advection of a cylinder of tracer in three dimensions by a 12 hour Sverdrup wave using PPM advection: (a) initial tracer value, (b) surface value at 3 hours, (c) surface value at 6 hours, (d) surface value at 9 hours, (e) surface value at 12 hours, (f) surface value at 24 hours, (g) section through the centre of the tracer ($x = 14$ km) at the initial time, (h) section at $x = 14$ km at 24 hours.

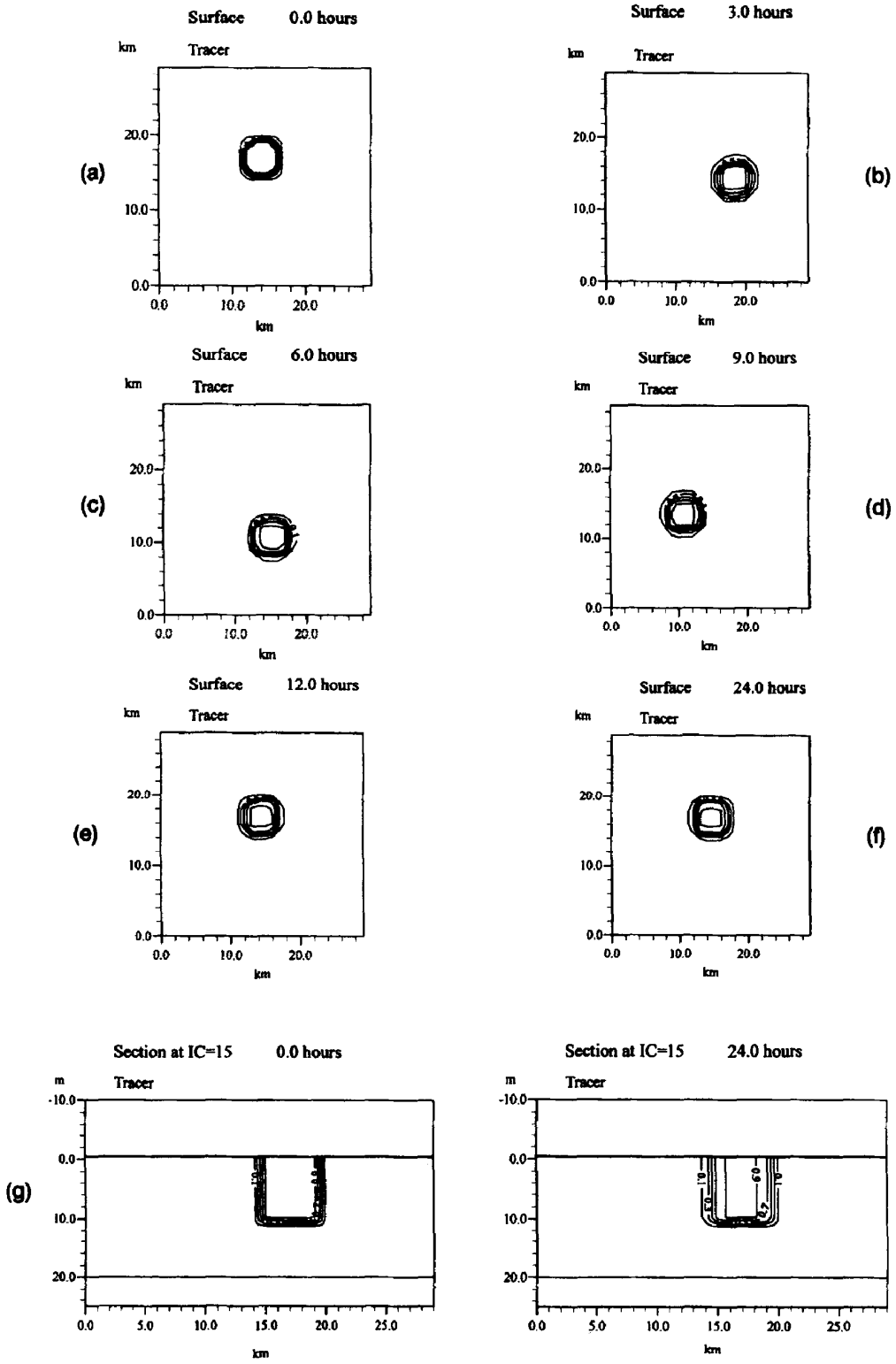
Surface 0.0 hours
km
Tracer
20.0
10.0
0.0
0.0
10.0
20.0
km
(a)
Surface 3.0 hours
km
Tracer
20.0
10.0
0.0
0.0
10.0
20.0
km
(b)
Surface 6.0 hours
km
Tracer
20.0
10.0
0.0
0.0
10.0
20.0
km
(c)
Surface 9.0 hours
km
Tracer
20.0
10.0
0.0
0.0
10.0
20.0
km
(d)
Surface 12.0 hours
km
Tracer
20.0
10.0
0.0
0.0
10.0
20.0
km
(e)
Surface 24.0 hours
km
Tracer
20.0
10.0
0.0
0.0
10.0
20.0
km
(f)
Section at IC=15 0.0 hours
m
Tracer
-10.0
0.0
10.0
20.0
0.0
5.0
10.0
15.0
20.0
25.0
km
(g)
Section at IC=15 24.0 hours
m
Tracer
-10.0
0.0
10.0
20.0
0.0
5.0
10.0
15.0
20.0
25.0
km
(h)

in the ratio $\omega/f$. In the examples shown here the elevation amplitude $Z$ is 0.5 m and the period of the wave is 12 hours. The horizontal resolution of the model is 1 km and there are 15 points in the vertical. The undisturbed depth $h$ is 20 m. The time steps used were 40 s (barotropic) and 400 s (baroclinic).

A cylindrical patch of tracer approximately 6 km in diameter and in the upper half of the water column is initially placed as shown in Fig. 5a. The tracer has value 1.0 in the centre of the patch, and decreases to zero horizontally as the eighth power of distance of the grid points from the centre, and vertically within one grid interval at the base, so giving sharp gradients. The section at coordinate IC = 15 (Fig. 5g) corresponds to a section through the centre of the patch at 14 km on the $x$ axis. The tracer patch is then advected by the tidal current. The results show, firstly, that the model run in frictionless mode successfully maintains the theoretical Sverdrup wave within this area. Figs. 5 and 6 show the results for the TVD and PPM schemes, respectively. Both schemes are monotonic, but the TVD scheme is clearly more diffusive, as we have already seen in one and two dimensions. Between the end of the first and second cycles, at 12 and 24 hours, the 0.7 contour is much reduced in extent for the TVD scheme, indicating continued diffusion. For the PPM scheme, however, there is very little difference between the results at 12 and 24 hours, and the 0.9 contour is retained. The section plots at 0 and 24 hours show how little diffusion there has been in the PPM case. These conclusions are also supported by the second moment calculations (Table 1).

### 6.3. Development of a freshwater eddy

In previous sections, we have considered only the passive advection of a tracer. Here, more dynamics is introduced by replacing the cylinder of tracer of section 6.2 by a cylinder of water of lower salinity than the ambient sea water. This has been modelled in the laboratory by Griffiths and Linden (1981), who released a cylinder of less dense water initially at rest relative to the rest of the fluid in a rotating tank. They found that the less dense fluid initially rises and spreads out at the surface, flowing anticyclonically. Fluid in the lower layer is drawn inwards and flows cyclonically. Within a time of order $1/f$ a quasi-geostrophic equilibrium state is reached, the initial radius of the eddy having increased by about one Rossby radius. For a two-layer fluid, the baroclinic Rossby radius is

$$R = (g'h')^{1/2}/f \tag{34}$$

where reduced gravity

$$g' = g(\rho_2 - \rho_1)/\rho_2 \tag{35}$$

and

$$h'h_1h_2/(h_1 + h_2) \tag{36}$$

where the density and depth of the upper layer are $\rho_1$ and $h_1$, and of the lower layer are $\rho_2$ and $h_2$.

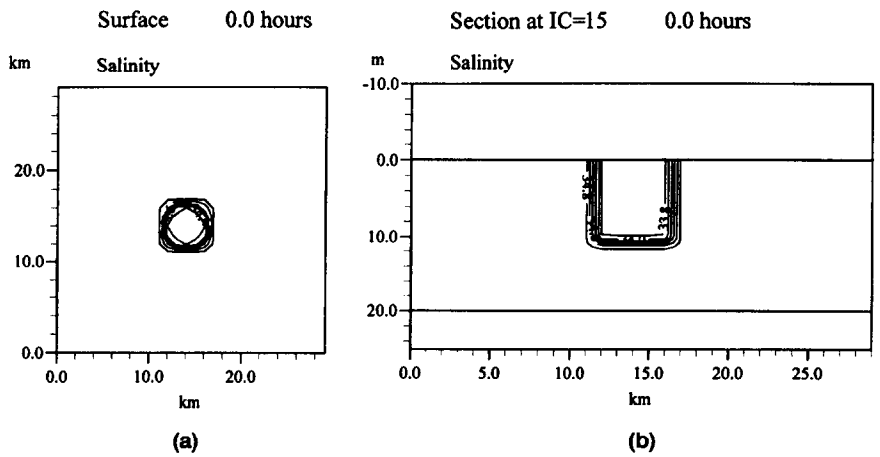


Fig. 7. Development of an eddy: (a) initial surface salinity, (b) initial section through the centre of the eddy.

Griffiths and Linden (1981) found that the vortices so formed were unstable, and that the zonal wavenumber of the instability depended on the initial parameters

$$\theta_0 = g' h_0 / f^2 R_0^2 \quad (37)$$

where $h_0$ is the initial depth of the cylinder of less dense water and $R_0$ its radius, and

$$\delta_0 = h_0 / H \quad (38)$$

where $H$ is the total depth.

To test the model, parameters which according to the experiments should give a wavenumber 2 instability, which is the easiest to resolve, were chosen. Dimensions of the cylinder are the same as in the tracer experiment in section 6.2, but salinities are 34.85 psu in the ambient sea water and 33.75 psu in the centre of the eddy. Temperature is fixed at 15°C. These parameter values imply that the initial radius $R_0$ of about 3 km is about twice the Rossby radius $R$ calculated from Eq. (34). The model experiment is begun from rest, as was the laboratory experiment. The same time steps were used as in section 6.2. The initial conditions are shown in Fig. 7.

After a period of adjustment involving inertial oscillations the modelled eddy shows the expected spreading and the development of anticyclonic circulation in the upper layer and cyclonic circulation in the lower layer. The model is also successful in demonstrating wavenumber 2 instability, as shown here at 144 hours in Figs. 8 and 9. (Column 15 corresponds to $x = 14$ km for salinity, through the centre of the eddy, but $x = 13.5$ km for velocity

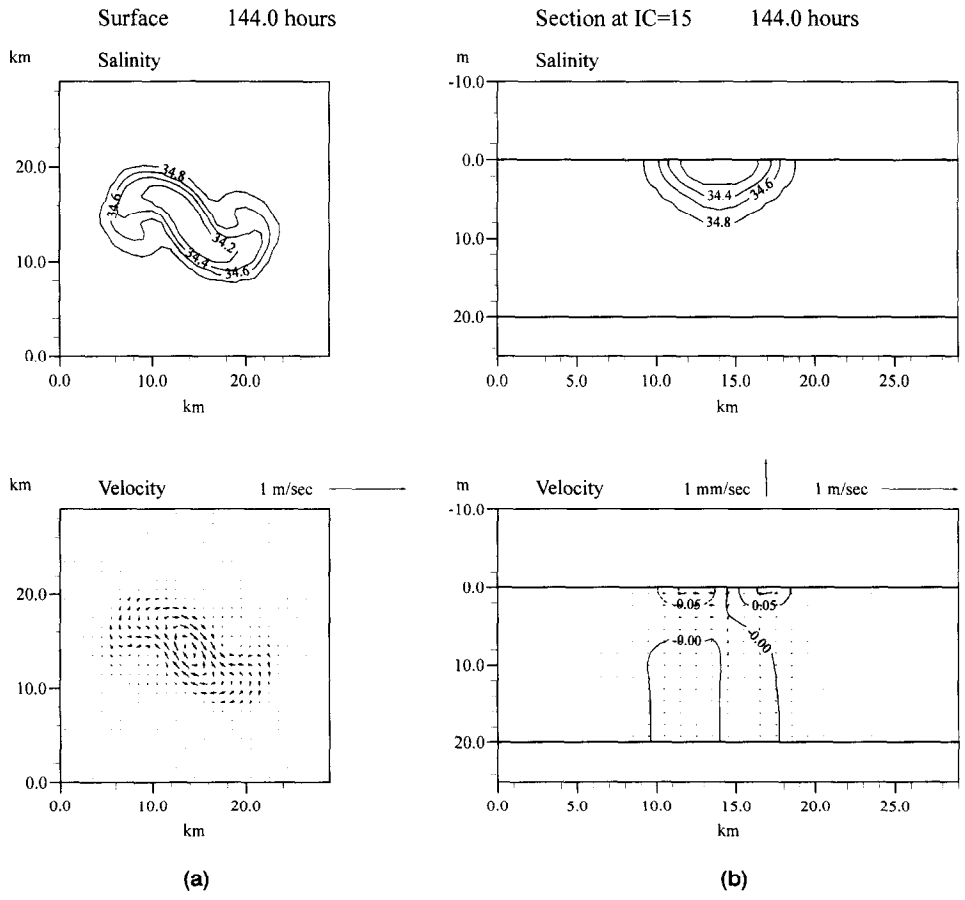


Fig. 8. The eddy after 144 hours, using TVD advection: (a) surface salinity and velocity, (b) section at column 15.

points). The anticyclonic surface motion has become elongated and cyclonic surface currents have appeared at each end, as in the laboratory experiments. Here we may focus on the differences between the result with TVD advection (Fig. 8) and with PPM advection (Fig. 9). It is clear that the results are qualitatively similar, with a similar orientation and size of the eddies, but that the PPM results are significantly sharper, with stronger fronts and higher velocities. The lower diffusion of PPM has produced a significant improvement at this relatively coarse resolution. The results for the upwind and Lax-Wendroff schemes are shown for comparison in Figs. 10 and 11. The upwind scheme shows more diffusion than TVD as expected, while the dispersive rippling of the Lax-Wendroff scheme gives an unacceptably irregular result. The four schemes are com-

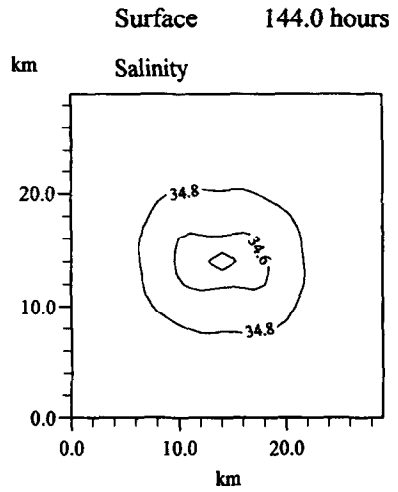


Fig. 10. Surface salinity for the eddy after 144 hours, using upwind advection.

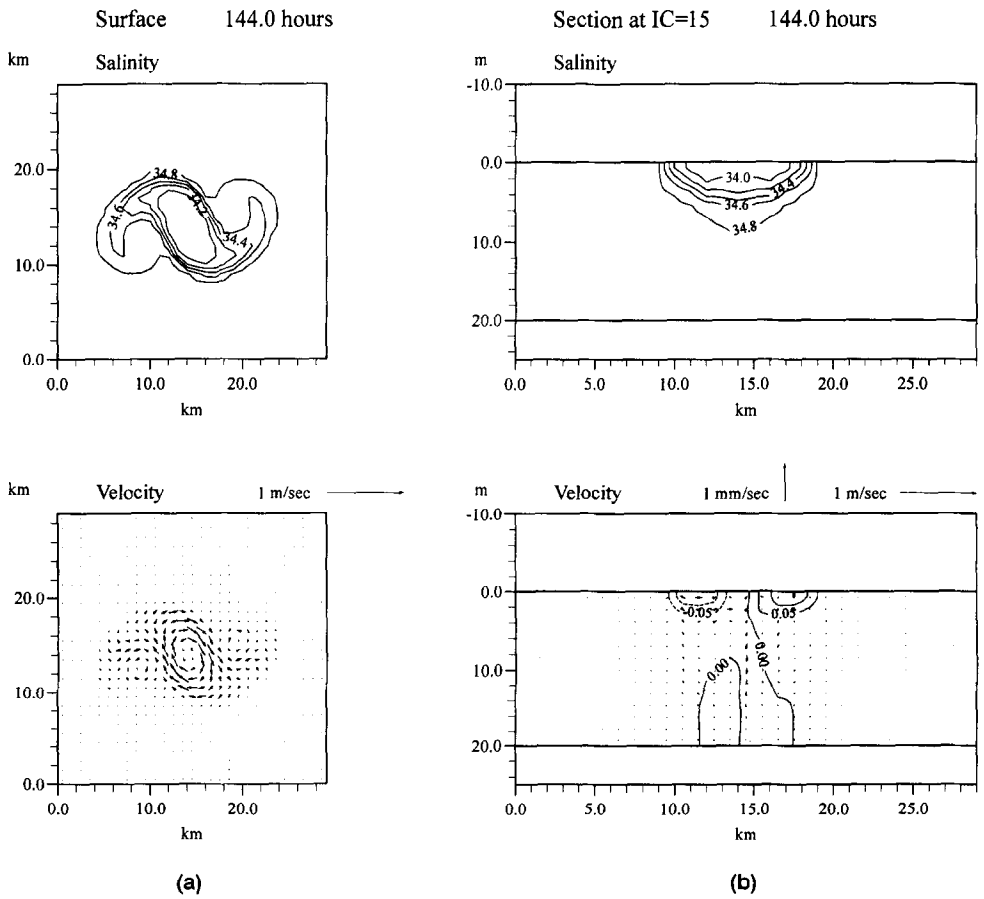


Fig. 9. The eddy after 144 hours, using PPM advection: (a) surface salinity and velocity, (b) section at column 15.

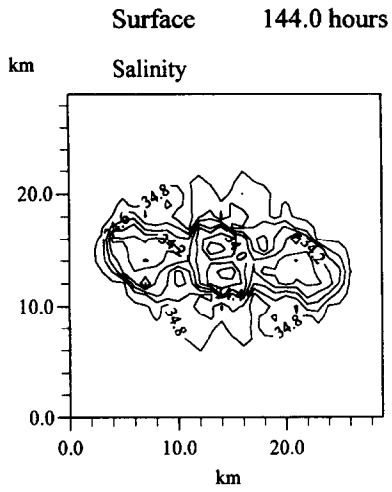


Fig. 11. Surface salinity for the eddy after 144 hours, using Lax-Wendroff advection.

pared in second moment calculations, based on a normalised salinity variable which has maximum value of 1 in the centre of the eddy and zero outside, in Table 1. This shows that the TVD scheme is more diffusive than PPM, while upwind is considerably more diffusive than TVD. The high values for Lax-Wendroff result from the unphysical ripples. PPM is more costly in computer time than TVD: it takes about 3 times the CPU time on a scalar workstation for the advection routine, but only approximately doubles the run time for the whole model, including momentum as well as scalar advection.

## 7. Conclusions

It has been shown that the TVD and PPM advection schemes described here offer monotonic performance with low diffusion for incompressible flow in one, two and three dimensions. They can be used satisfactorily in sigma coordinates, where schemes with low diffusion are needed to minimise artificial vertical diffusion of thermoclines over sea bed slopes. Their use has been demonstrated in a three-dimensional hydrodynamic model of a freshwater eddy, which reproduces behaviour found in laboratory experiments.

The PPM scheme is significantly less diffusive than the TVD scheme used here, although it involves more computation time. The PPM scheme therefore seems particularly suitable for shelf sea models in which advection of sharp gradients, in thermoclines, fronts and eddies, or of tracers, is important.

## Acknowledgements

This work was partly funded under contract to the UK Department of the Environment as part of its coordinated programme of research on the North Sea. It was also supported by the EC through the MAST programme under contract MAS2-CT930054.

I would like to thank an anonymous referee for suggesting the use of integrated second moments to compare numerical diffusion.

## References

Beckers, J.-M., 1991. Application of GHER 3D general circulation model to the western Mediterranean. J. Mar. Syst., 1: 315–332.

Boris, J.P. and Book, D.L., 1976. Solution of continuity equations by the method of flux-corrected transport. Methods Comput. Phys., 16: 85–129.

Carpenter, R.L., Droegemeier, K.K., Woodward, P.R. and Hane, C.E., 1990. Application of the piecewise parabolic method (PPM) to meteorological modelling. Mon. Weather Rev., 118: 586–612.

Colella, P. and Woodward, P.R., 1984. The piecewise parabolic method (PPM) for gas-dynamical simulations. J. Comput. Phys., 54: 174–201.

Griffiths, R.W. and Linden, P.F., 1981. The stability of vortices in a rotating, stratified fluid. J. Fluid Mech., 105: 283–316.

Harten, A., 1978. The artificial compression method for computation of shocks and contact discontinuities: III-Self-adjusting hybrid schemes. Math. Comput., 32: 363–389.

Harten, A., 1983. High resolution schemes for hyperbolic conservation laws. J. Comput. Phys., 49: 357–393.

James, I.D., 1986. A front-resolving sigma coordinate sea model with a simple hybrid advection scheme. Appl. Math. Modelling, 10: 87–92.

James, I.D., 1990. Numerical modeling of density-driven circulation in shelf seas. In: A.M. Davies (Editor), Modeling Marine Systems. CRC Press, Boca Raton, FL, 2, pp. 345–372.

Killworth, P.D., Stainforth, D., Webb, D.J. and Paterson, S.M., 1991. The development of a free-surface Bryan-Cox-Semtner ocean model. J. Phys. Oceanogr., 21: 1333–1348.

Leonard, B.P., 1988. Simple high-accuracy resolution program for convective modelling of discontinuities. Int. J. Numer. Methods Fluids, 8: 1291–1318.

Press, W.H., Teukolsky, S.A., Vetterling, W.T. and Flannery,

B.P., 1992. Numerical Recipes. Cambridge Univ. Press, Cambridge, 2nd ed., 992 pp.

Roe, P.L., 1986. Characteristic-based schemes for the Euler equations. Ann. Rev. Fluid Mech., 18: 337–365.

Smolarkiewicz, P.K., 1983. A simple positive definite advection scheme with small implicit diffusion. Mon. Weather Rev., 111: 479–486.

Souza, A.J. and James, I.D., 1996. A two-dimensional (x-z) model of tidal straining in the Rhine ROFI. Cont. Shelf Res., 116: 949–966.

Sweby, P.K., 1984. High resolution schemes using flux limiters for hyperbolic conservation laws. SIAM J. Numer. Anal., 21: 995–1011.

Van Leer, B., 1979. Towards the ultimate conservative difference scheme, V. A second-order sequel to Godunov's method. J. Comput. Phys., 32: 101–136.

Yang, H.Q. and Przekwas, A.J., 1992. A comparative study of advanced shock capturing schemes applied to Burgers' equation. J. Comput. Phys., 102: 139–159.